

A large scale extinction map of the Galactic Anticenter from 2MASS

D. Froebrich^{1,3*}, G.C. Murphy^{2,3}, M.D. Smith¹ and J. Walsh⁴

¹ Centre for Astrophysics and Planetary Science, University of Kent, Canterbury, CT2 7NH, UK

² Laboratoire d'Astrophysique, Observatoire de Grenoble, BP 53, 38041 Grenoble Cedex 9, France

³ Dublin Institute for Advanced Studies, 5 Merrion Square, Dublin 2, Ireland

⁴ School of Computer Science and Statistics, Trinity College, College Green, Dublin 2, Ireland

Received sooner; accepted later

ABSTRACT

We present a $127^\circ \times 63^\circ$ extinction map of the Anticenter of the Galaxy, based on $\langle J - H \rangle$ and $\langle H - K \rangle$ colour excess maps from 2MASS. This 8001 square degree map with a resolution of 4 arcminutes is provided as online material. The colour excess ratio $\langle J - H \rangle / \langle H - K \rangle$ is used to determine the power law index of the reddening law (β) for individual regions contained in the area (e.g. Orion, Perseus, Taurus, Auriga, Monoceros, Camelopardalis, Cassiopeia). On average we find a dominant value of $\beta = 1.8 \pm 0.2$ for the individual clouds, in agreement with the canonical value for the interstellar medium. We also show that there is an internal scatter of β values in these regions, and that in some areas more than one dominant β value is present. This indicates large scale variations in the dust properties. The analysis of the A_V values within individual regions shows a change in the slope of the column density distribution with distance. This can either be attributed to a change in the governing physical processes in molecular clouds on spatial scales of about 1 pc or an A_V dilution with distance in our map.

Key words: ISM: clouds – ISM: dust, extinction – Galaxy: structure– Infrared: ISM

1 INTRODUCTION

Understanding the formation of stars is inextricably linked to the formation, evolution and physical properties of molecular clouds. Dust is one of the best tracers of the distribution of material in giant molecular clouds. Its optical properties (reddening and dimming of star light) allow us to determine line of sight column densities of material. The knowledge of how clouds are structured (e.g. the distribution of mass, size and column density of clumps within clouds) can be used to obtain constraints about how clouds fragment and will eventually lead to a better understanding of the initial mass function (e.g. Padoan, Nordlund, & Jones (1997)).

The mapping of the dust distribution in giant molecular clouds or entire cloud complexes becomes increasingly achievable due to the availability of all sky near infrared surveys such as 2MASS (Skrutskie et al. (2006)) as well as large computer clusters and Grid technology. Basic techniques to map the column density of dust, i.e. extinction, are: 1) star counting (e.g. Wolf (1923), Bok (1956), Froebrich et al. (2005)); 2) colour excess (e.g. Lada et al. (1994), Lombardi & Alves (2001)); 3) or a combination thereof (e.g. Lombardi (2005)); While most simple, the star counting techniques suffer from enhanced noise compared to the colour excess techniques, when applied to near infrared data. On the other hand, using colour excess methods to determine extinction requires the knowledge of

the reddening law, which might vary with position and/or column density (e.g. Froebrich & del Burgo (2006)). In this paper we apply the most basic colour excess method from Lada et al. (1994) and determine the reddening law in the near infrared following Froebrich & del Burgo (2006).

A large fraction of nearby giant molecular clouds is part of the Gould Belt. Towards the Anticenter of the Galaxy we find a variety of these clouds (e.g. Perseus, Taurus, Orion) in relative close proximity and with a relatively small amount of contamination from other clouds in the Galactic Plane. Additionally, a number of more distant cloud complexes (e.g. Cassiopeia, Camelopardalis, Auriga, Monoceros) are found in the same part of the sky. We hence selected an area of $127^\circ \times 63^\circ$ (in Galactic Coordinates) towards the Galactic Anticenter to be mapped in detail and to investigate the column density distribution in the major cloud complexes situated in this region.

The paper is structured as follows. In Sect. 2 we describe our method to determine the extinction map. A description and discussion of the determination of the reddening law is given in Sect. 3. Finally we study the distribution of column densities in Sect. 4, followed by the conclusions in Sect. 5.

* E-mail: df@star.kent.ac.uk

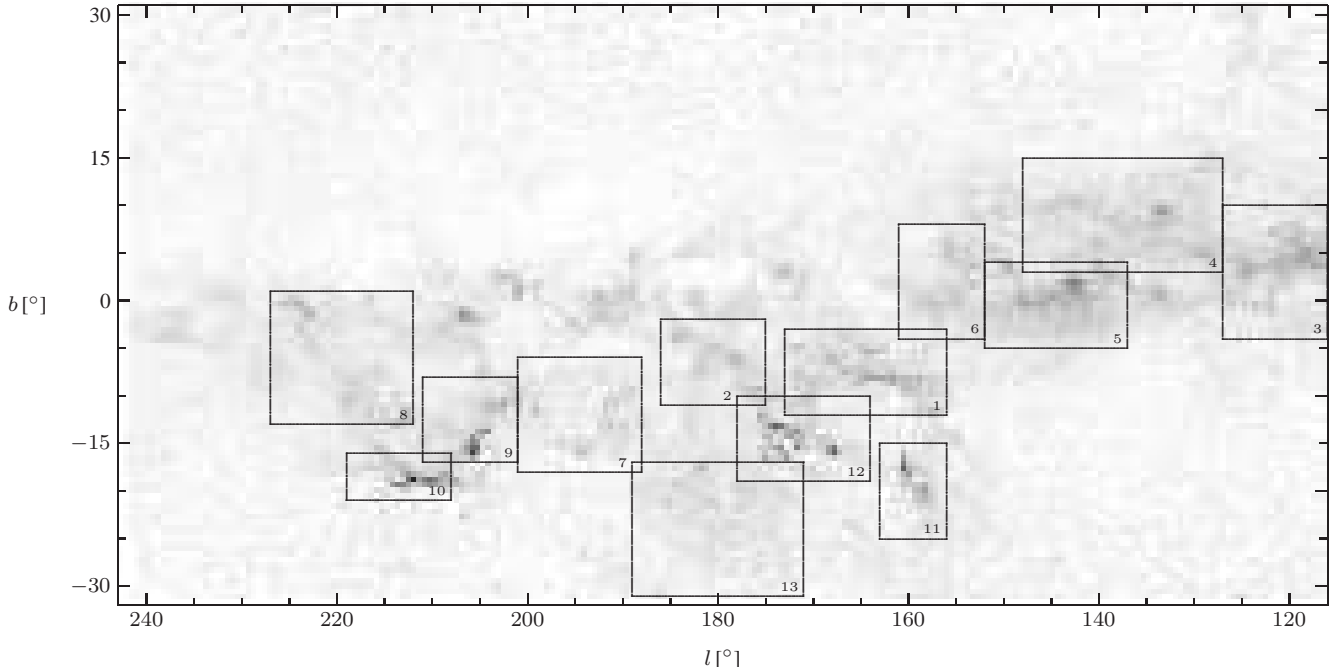


Figure 1. Gray scale illustration of our 8001 square degrees extinction map of the Galactic Anticenter obtained from $\langle J - H \rangle$ and $\langle H - K \rangle$ colour excess determinations in 2MASS. Pixel values are scaled linearly from -0.33 mag to 10 mag optical extinction. The rectangles mark the regions selected for detailed analysis (numbers are identical to their ID in Table 1), and magnified extinction maps of these areas can be found in Appendix A1. The full resolution FITS file of this map is available as online material.

2 THE EXTINCTION MAP

We selected all objects from the 2MASS point source catalogue with a Galactic Longitude of $116^\circ < l < 243^\circ$ and a Galactic Latitude of $-32^\circ < b < +31^\circ$. To ensure good photometric accuracy only objects with a quality flag better than 'E' are used. The area was then decomposed into $1^\circ \times 1^\circ$ sized regions. Independent of the position we determined the median colour of stars ($J - H$ and $H - K$) in $4' \times 4'$ sized boxes with an oversampling of 2. This leads to a pixel size of $2'$, 30×30 pixels per square degree, or 3810×1890 pixel for our 8001 square degree sized final map. The calculations required for such a project are embarrassingly parallel (i.e. the problem domain and the associated computational algorithms used to solve this problem can be optimally decomposed to use the available computer resources) and have been solved in a distributed fashion. We used the Grid-Ireland infrastructure (e.g. Coghlan et al. (2005)) to perform these calculations.

The correct determination of extinction from colour excess methods requires that we remove the foreground stars to the cloud and that we reject young stellar objects. Both types of objects systematically influence the determined extinction values. Foreground stars lead to on average bluer colours, hence the extinction is underestimated. Young stars are intrinsically red and hence lead to an overestimate of the extinction. Due to the large range of distances of the clouds in our map (ranging from 140 pc to at least 1 kpc) the removal of foreground stars is very difficult. In principle the number of foreground stars has to be evaluated for each individual cloud and removed statistically. The large number of clouds in the map with partly unknown distances, or overlapping clouds close to the Galactic Plane makes this an almost impossible task. However, if the stars in each box are not dominated by foreground objects and one uses the median colour of stars instead of the average, then the foreground stars are removed automatically. Froebrich & del Burgo

(2006) have shown (see their Fig. 9) that such an approach indeed reproduces the intrinsic extinction values of clouds extremely well, as long as the cloud is not too distant, or has a very high extinction. For very distant clouds or very high extinction regions, however, this approach detects zero extinction. Hence, locally more sophisticated procedures such as described in Lombardi (2005) or suggested in Froebrich & del Burgo (2006) have to be used to obtain correct extinction values for the highest extinction regions. Since only a very small portion of the map area is affected and we are investigating only the large scale distribution of clouds and their properties in this paper, the main conclusions of this paper are not significantly changed by this effect. However, when using the presented extinction map one has to keep in mind that the extinction values in the very dense regions of clouds are underestimated and that there is a small A_V dilution for more distant clouds. Similarly to the removal of foreground stars, the use of the median colour also removes intrinsically red YSOs, as long as they do not dominate (as e.g. in the Orion Nebula cluster).

The two median $J - H$ and $H - K$ colour maps of the entire field show small but significant large-scale gradients of the colour values of background (i.e. extinction free) regions. These gradients are caused by a change of the stellar population with distance from the Galactic Plane. In particular, the median colour of stars becomes bluer at lower Galactic Latitudes and (less prominent) redder towards Galactic Longitudes approaching the Anticenter of the Galaxy. To determine the $\langle J - H \rangle$ and $\langle H - K \rangle$ colour excess maps, we thus fitted a polynomial of 3rd order in l and b to the extinction free regions and subtracted it from the median colour maps.

The resulting $\langle J - H \rangle$ and $\langle H - K \rangle$ colour excess maps are converted separately into H-band extinction maps using Equ. 8 and 9 of Froebrich & del Burgo (2006), respectively. A power law index

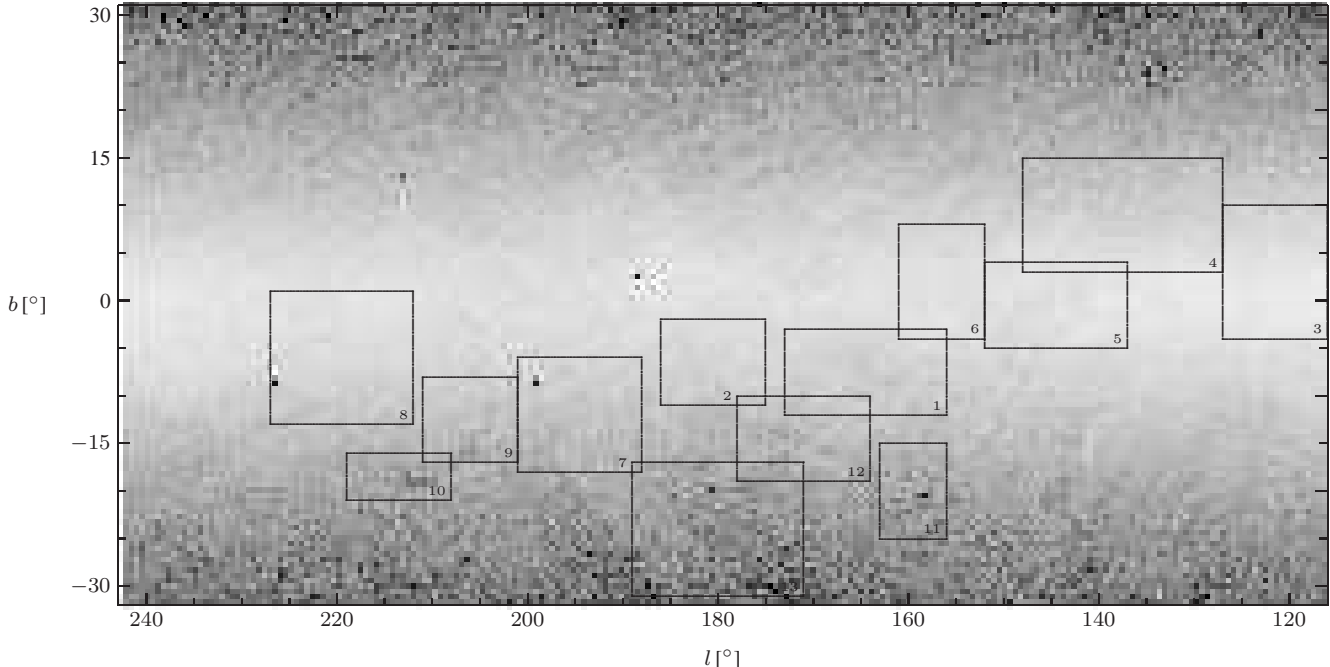


Figure 2. Gray scale illustration the noise map. Pixel values show the one sigma noise level scaled linearly from 0.0 mag (white) to 0.6 mag (black) of optical extinction. The rectangles mark the regions selected for detailed analysis (numbers are identical to their ID in Table 1)

of the reddening law of $\beta = 1.73$ is applied (see Sect. 3 for details). The resulting two H-band extinction maps are averaged and converted into our final optical extinction map by $A_V = 5.689 \times A_H$, using the reddening law from Mathis (1990). In Fig. 1 we show this map in gray-scale. Indicated in this figure are the regions of which we show magnified versions of the extinction map in Appendix A1. These are also the regions we analyse in detail in the forthcoming sections. The full resolution FITS version of our entire map will be provided as online material to this paper. Note that the construction of the final extinction maps as average of the A_H extinction maps from $\langle J - H \rangle$ and $\langle H - K \rangle$ colour excess maps leads to further dilution of the very high extinction cores. This will, however, effect the same areas that are dominated by foreground stars, as described above. Thus, the number of high column density regions in our analysis will be underestimated.

The noise in the extinction map can in principle only be measured in extinction free regions as the standard deviation of extinction values from zero. To estimate the noise in all areas we have determined a noise map (see Fig. 2). Since we used the median colour of stars in each pixel, we need to determine the standard error of the median for our noise map. For a large sample and normal distribution this can in principle be done by $\sigma_{med} = 1.25 \cdot \sigma / \sqrt{N}$, where σ is the error of the colour of the individual stars and N the number of stars in each box. Since we use stars of different photometric quality (see below) and we do not know if the sample of stars in each pixel follows a normal distribution, we cannot use this equation. However, the fraction of stars for any given photometric quality is very constant (see below). Thus, we can conclude that the noise in each pixel is proportional to $1/\sqrt{N}$ for both, the $\langle J - H \rangle$ and $\langle H - K \rangle$ maps. We have thus scaled and co-added the $1/\sqrt{N}$ maps of stars with (J and H) and (H and K) photometry, in order to obtain the final noise map. The scaling was done to match the measured noise in the A_V map in extinction free regions. As can be seen, the noise in the map varies significantly with Galactic Latit-

tude, as well as with extinction. The 3σ noise ranges from 0.36 mag optical extinction, close to the Galactic Plane, to 1.0 mag A_V in the most northern and southern parts of the map as well as in high extinction regions. In Table 1 we list for all individual regions the average number of stars with detections in J and H, as well as the average noise in the area. There are pixels in the map (0.0066 %) where the noise is extremely large, i.e., there are no stars to determine the colour. These regions are: 1) around very bright stars; 2) at $|b| > 30^\circ$; 3) high extinction cores in Orion, Taurus, Perseus. For Ori A we determine an average noise of 0.24 mag, which can be compared to the 1σ noise level of about 0.2 mag A_V obtained by Lombardi & Alves (2001) (see their Fig. 6) in this region using the optimised NICER method.

There are further areas in the map where the extinction values are not very reliable. These are positions close to dense star clusters. Here, the high number of stars in the cluster dominates the extinction determination. Hence, depending on the colour of the cluster members we measure either a too low (mostly blue stars) or too high (mostly young, red stars) extinction. Since this is a common effect, we over plotted circles at the positions of all known star clusters (found in SIMBAD) in the gray scale maps of our selected regions in Appendix A1. Additionally we over plot + signs at the positions of all possible new star clusters with $|b| < 20^\circ$ found by Froebrich et al. (2007).

Does the use of 2MASS quality BCD stars instead of only quality A stars influence the noise in our map? Independent of the position about 40–45 % of all stars are of quality AAA. Given the larger errors in photometry for the quality BCD objects, one can estimate that the noise in the extinction map is about 10 % (i.e. 0.03 mag) higher, when including the lower quality objects. However, as has been pointed out by Froebrich & del Burgo (2006), systematic errors of extinction determinations based on colour excess methods can be much higher than this, since the population of stars seen through a cloud can differ from the population of stars

in a control field (even if close-by). The more than twice as large number of stars per resolution element when including the lower quality objects will lead to a much better representation of the population of stars and, as a result, to smaller systematic errors. This out weights in our opinion the slightly higher resulting statistical noise in our maps and justifies the use of the lower quality 2MASS sources.

Note that the galaxies M 31 ($l=121.2$, $b=-21.6$) and M 33 ($l=133.6$, $b=-31.3$) show up as apparently high extinction regions. In M 31 the structure in our extinction map resembles quite closely the $170\mu\text{m}$ emission map from Haas et al. (1998) and in particular we are able to identify the dominant ring of material in the disc of the Andromeda Galaxy.

3 THE REDDENING LAW

The conversion of colour excess maps into extinction maps requires the knowledge of the extinction law. Our approach of using $\langle J - H \rangle$ and $\langle H - K \rangle$ colour excess maps enables us to determine the power law index of the extinction law using the colour excess ratio $R \equiv \langle J - H \rangle / \langle H - K \rangle$ and

$$0 = \left(\frac{\lambda_2}{\lambda_1} \right)^\beta + R \cdot \left(\frac{\lambda_3}{\lambda_2} \right)^{-\beta} - R - 1 \quad (1)$$

from Froebrich & del Burgo (2006). We now can analyse the resulting distribution of β values in our maps. For all the following analysis of β we use only areas where both, the $\langle J - H \rangle$ and $\langle H - K \rangle$ colour excess values are 3σ above the noise. In Fig. 3 we show the histogram of the measured distribution of all β values ($N_o(\beta)$) as dotted line. It peaks at 1.73, in good agreement with the canonical value for the interstellar medium (Draine (2003)). We hence use $\beta = 1.73$ to convert our colour excess maps into extinction. The distribution of β values shows a rather broad peak with a FWHM of 1.6. This, seemingly, rather large value is in good agreement for the predicted scatter of about $\pm 40\%$ when using the colour excess ratio to determine β (see e.g. Fig. 1 in Froebrich & del Burgo (2006)).

It is possible to investigate in more detail, if the measured distribution of β values $N_o(\beta)$ is in agreement with a single value of $\beta_0 = 1.73$ in the entire field or not. This can be done by convolving the observed distribution of signal to noise values, $N_o(\langle J - H \rangle)$, in our extinction map from Fig. 1 with the predictions for the width of the distribution of β . We have, however, to allow for the possibility that there is an intrinsic scatter in the β values ($\sigma_{\beta_{int}}^2$) around β_0 . We hence have to adapt Equ. 11 from Froebrich & del Burgo (2006) and obtain:

$$\sigma_\beta^2 = \frac{\sigma_{\langle \lambda_1 - \lambda_2 \rangle}^2}{(\lambda_1 - \lambda_2)^2} R^2 \left[1 + \frac{R^2}{\alpha_{co}} - 2 \frac{R}{\gamma_{co}} \right] \left(\frac{\partial \mathbf{B}(R)}{\partial R} \right)^2 + \sigma_{\beta_{int}}^2 \quad (2)$$

To determine the predicted distribution of β values we use:

$$N_p(\beta) = N_0 \int N_o(\langle J - H \rangle) \cdot e^{-\frac{1}{2} \left(\frac{\beta - \beta_0}{\sigma_\beta(\langle J - H \rangle)} \right)^2} \cdot d\langle J - H \rangle \quad (3)$$

where N_0 is a normalisation factor and $\beta_0 = 1.73$ the peak of the measured β distribution. A Kolmogorov Smirnov test can then be performed with $N_o(\beta)$ and $N_p(\beta)$ to determine the probability (P) that the two distributions are drawn from the same sample.

In order to determine the predicted β distribution we require

to estimate the parameters α_{co} and γ_{co} . The parameter α_{co} represents the square of the ratio of the noise in the two colour excess maps and γ_{co} represents the ratio of the square of the noise in one colour excess map and the covariance of the two colour excess maps (see Equ. 2 and Froebrich & del Burgo (2006) for details). For our dataset we measure values of: $\alpha_{co} = 3.6$ and $\gamma_{co} = 3.7$. Note that the values for both parameters might slightly vary with position or hence from cloud to cloud. However, we have measured here the same values for α_{co} and γ_{co} as were obtained for 2MASS data in IC 1396 W by Froebrich & del Burgo (2006). Due to this fact, and since the dependence of the predicted β distribution on α_{co} and γ_{co} is rather weak, we fix these values for all our determinations.

This gives us the possibility to vary the intrinsic scatter $\sigma_{\beta_{int}}^2$ and the β_0 value until we find the highest probability P that the observed and predicted distributions of β values match. We list the obtained values of those parameters as well as the probabilities for the individual regions in Table 1.

We over plot the resulting best predicted distribution for β values of the entire field as solid line in Fig. 3. We find that with a 98.9 % probability the two distributions are equal, when a value of $\beta_0 = 1.73$ and an intrinsic scatter of $\sigma_{\beta_{int}}^2 = 0.52$ is assumed. The large intrinsic scatter shows, that there is a good chance that indeed variable β values are present in different parts of the field. Hence, repeating the same analysis for selected regions should lead to different β values in different clouds. If locally those clouds have more uniform dust properties, then a lower intrinsic scatter should be found.

Thus, similar to the entire area, we investigate the peak value of the β distribution, the intrinsic scatter and how well the distribution matches the assumption of a constant β value for our individual regions. In Table 1 we summarise the obtained results. We find an average value of $\beta = 1.8 \pm 0.2$. Almost in all investigated regions the β value is in agreement with the estimate for the entire field. Only in Auriga 2 ($\beta = 2.05$), Monoceros ($\beta = 1.52$) and Camelopardalis 2 ($\beta = 1.40$) significantly different values are found, hinting to different dust properties such as the grain size distribution in these areas. Notably, regions with smaller β values tend to be closer to the Galactic Plane. However, it is not clear if this is caused by different dust properties or by the overlap of clouds in this area. Furthermore, small systematic off-sets in either $\langle J - H \rangle$ or $\langle H - K \rangle$ can cause changes in the determined β value. Thus, the procedure of fitting a polynomial to the extinction free regions in order to determine the colour excess maps might also contribute to these smaller β values. Since very close to the Galactic Plane there are no extinction free regions, the procedure might have introduced a small off-set in the colour excess maps and hence to the β values. Clearly, more detailed investigations are required to find the cause of the smaller β values very close to the Galactic plane.

We also find that for most regions the intrinsic scatter of the β values is smaller or in the order of the value for the entire field. Only in Ori A is a significantly larger value found. The probabilities that measured and predicted values are drawn from the same sample are listed in Table 1 and the individual distributions are shown in Appendix A2. We find that in some regions the proposal of constant β values with the corresponding internal scatter is more probable than in others. Especially in the regions Monoceros and Ori B low probabilities ($P < 95\%$) are found. We can conclude that in these regions we do not see a dominant fraction of the dust possessing constant optical properties. This might indicate large scale variations of the optical dust properties within these clouds.

Table 1. Names and areas of our individual regions, average numbers of stars in the $4' \times 4'$ box, average noise in the field, peak in the distribution of β , intrinsic scatter of the β distribution, probability that the measured distribution is in agreement with the predicted one for the assumption of a constant β_0 value and intrinsic scatter in the whole region and slope of the column density distribution in the $\log N$ vs. A_V plot.

ID	Name	l -range	b -range	#stars/box	σ_{A_V} [mag]	β_0	$\sigma_{\beta_{intr}}$ [mag]	P [%]	slope
1	Auriga 1	156 – 173	–12 – –03	47	0.15	1.99	0.45	98.5	-0.68
2	Auriga 2	175 – 186	–11 – –02	53	0.14	2.05	0.39	99.9	-0.83
3	Cassiopeia	116 – 127	–04 – +10	90	0.11	1.67	0.43	99.9	-0.72
4	Camelopardalis 1	127 – 148	+03 – +15	53	0.15	1.96	0.49	98.4	-0.91
5	Camelopardalis 2	137 – 152	–05 – +04	78	0.12	1.40	0.54	98.5	-0.71
6	Camelopardalis 3	152 – 161	–04 – +08	74	0.12	1.66	0.49	95.2	-1.20
7	λ -Ori	188 – 201	–18 – –06	36	0.18	1.87	0.24	96.3	-0.81
8	Monoceros	212 – 227	–13 – +01	67	0.14	1.52	0.53	82.7	-0.68
9	Orion B	201 – 211	–17 – –08	34	0.18	1.77	0.41	91.2	-0.38
10	Orion A	208 – 219	–21 – –16	20	0.24	1.66	0.59	99.8	-0.28
11	Perseus	156 – 163	–25 – –15	18	0.25	1.97	0.51	99.9	-0.30
12	Taurus	164 – 178	–19 – –10	27	0.20	1.99	0.47	99.9	-0.32
13	Taurusextended	171 – 189	–31 – –17	14	0.29	1.92	0.43	99.9	-0.49
14	Entire Field	116 – 243	–32 – +31	—	—	1.73	0.52	98.9	—

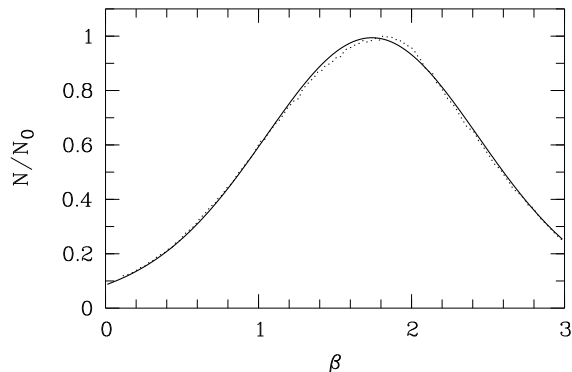


Figure 3. Histogram of the distribution of β values in the entire field (dotted line) measured for all pixels where the $\langle J - H \rangle$ and $\langle H - K \rangle$ colour excess values are at least 3σ above the noise. The solid line represents the predicted distribution for a value of $\beta=1.73$, $\sigma_{\beta_{intr}}=0.52$ and the measured distribution of A_V values in the entire field (see text for details). A Kolmogorov Smirnov test shows that both distributions are identical with a probability of 98.9 %.

4 THE COLUMN DENSITY DISTRIBUTION

In order to analyse and interpret the distribution of column density values in the entire map, as well as in the individual regions, we first have to recapitulate the selection effects induced by our method. As outlined in detail in Sect. 2, our method of determining the extinction maps leads to three biases. (1) Very distant clouds, as well as very high extinction regions will not be detected by our method, since these areas are dominated by foreground stars. (2) There is a small A_V dilution with distance. (3) The averaging of extinction maps from $\langle J - H \rangle$ and $\langle H - K \rangle$ colour excess maps leads to dilution of the high extinction cores. (4) Regions close to rich star clusters will be dominated by the colours of the cluster members. However, due to the use of the median stellar colours instead of the mean colours, all not too distant clouds without rich clusters and extremely dense cores, will have no systematically influenced extinction values.

The general way of analysing the structure of molecular clouds is to determine the distribution of clumps within them. This

includes the clump mass, size and column density distribution. We have hence used the *clumpfind-2D* algorithm (Williams et al. (1994)) to extract all detectable clumps in our final extinction map and determined their size and mass distribution. Contrary to line or dust emission maps, extinction maps have real, very smooth large scale profiles which make it very difficult to extract structure information using an automated thresholding technique. This is reflected by the fact that the determined clump properties from our map depended, partly significantly, on the chosen levels and also on the pixel size of the map.

Hence, instead of using the clump properties in the map, we will analyse the column density distribution in the individual regions. Since the distance of the clouds will influence the measured slope of the column density distribution (see below), we will not analyse the distribution of the entire map as a whole. We show in Appendix A2 the A_V distributions for all individual regions (solid line). For each region we fit a linear polynomial to the $\log(N)$ vs. A_V plots (dashed line) for extinction values larger than the 5σ noise (vertical line). The measured slopes are indicated in the individual diagrams as well as in Table 1.

The individual A_V distributions nicely show the above discussed biases for high extinction values. Some show a clear drop-off for regions with very high column densities. Depending on the distance of the cloud and its position, this drop-off occurs at different values. For Ori A and Ori B we see a clear drop at $A_V = 10$ mag, while for Perseus ($A_V = 8$ mag) and Camelopardalis 2 ($A_V = 6$ mag) lower values are found. The values of the slopes range from about -0.3 to almost -1.0, with the exception of Camelopardalis 3 where -1.2 is found.

The interpretation of these values is, however, rather difficult. Two effects could influence the measured slope: (1) the distance of the cloud; (2) the intrinsic distribution of material. The distance could influence the slope since in more distant clouds the extinction per resolution element is averaged over a larger physical area in the cloud. Hence, for more distant clouds the column density distribution on larger physical scales is measured. One can artificially move a cloud to larger distances by using a larger box-size for the extinction measurements. Indeed one finds that this results in a steeper column density distribution. This is in agreement with the values obtained from our data, where more distant clouds possess on average steeper column density distributions. We basically

6 Froebrich, Murphy, Smith & Walsh

find that in all clouds where our resolution element is smaller than 1 pc the slope of the distribution is -0.3. For all clouds where we are not able to resolve 1 pc (cloud distance larger than 850 pc) the slope in the column density distribution is about -0.75. This leads to the conclusion that there might be a change in the governing physics determining the column density distribution in molecular clouds on a scale of about 1 pc. Interestingly, this is about the Jeans length for a column density that is required for self-shielding and molecular hydrogen formation in molecular clouds (Hartmann et al. (2001)). The already discussed small A_V dilution with distance could as well contribute to the change in the slope. Furthermore, there could also be intrinsic differences between clouds, as reflected by the different slopes measured for e.g. Ori A and Ori B, which are believed to be at the same distance. We note however, that if measured only for $b < -13^\circ$ the slope for Ori B is -0.32, hence in very good agreement with Ori A and the other close-by clouds Taurus and Perseus. For the region with $b > -13^\circ$ in Ori B the slope is -0.75, indicating that these clouds are more distant. We further note that an overlap of different clouds, as may happen close to the Galactic plane, does not change the measured slope if the individual clouds are at about the same distance and have intrinsically the same slope.

5 CONCLUSIONS

Using Grid technology and 2MASS data we created the largest extinction map to date based on near infrared colour excess. Our $127^\circ \times 63^\circ$ sized map of the Galactic Anticenter contains the molecular cloud complexes of Orion, Taurus, Cepheus, Monoceros, Auriga, Camelopardalis and Cassiopeia. The three sigma noise level ranges from 0.36 mag optical extinction close to the Galactic Plane to 1.0 mag A_V at $|b| \approx 30^\circ$ and in high extinction regions. Our final optical extinction map has a resolution of 4' and a pixel size of 2'.

The colour excess ratio $\langle J - H \rangle / \langle H - K \rangle$ is used to determine the power law index β of the wavelength dependence of the extinction in the near infrared. In the entire field the distribution of β peaks at a value of 1.73. The average value of the investigated cloud complexes is determined to $\beta = 1.8 \pm 0.2$. Both values are in agreement with the assumed values for the interstellar medium. We analyse in detail the distribution of β values in the entire field and individual regions. It is found that there is an internal scatter in the β values of about 0.4–0.5. A comparison of the measured and predicted β distribution by means of a Kolmogorov Smirnov tests shows that in most regions the proposal of a constant β with an internal scatter is valid. In some regions (e.g. Monoceros, Ori B) low probabilities that observations and predictions match are found. Hence, there is no dominant β value in the cloud, a clear indication of large scale variations of the optical dust properties in these areas.

We further analysed the column density distribution of the individual regions. Due to our technique, the highest extinction cores ($A_V > 10$ mag) cannot be identified reliably. For extinction values up to 10 mag A_V we find that the column density distributions show a linear behavior in the $\log(N)$ vs. A_V plot. On average a steeper column density distribution for more distant clouds is found, i.e. the A_V distribution is steeper when measured on larger spatial scales. This seems to indicate a change in the governing physics of the column density at scales of about 1 pc or an A_V dilution with distance in our map.

ACKNOWLEDGMENTS

We are grateful to the anonymous referee for helpful comments which significantly improved the paper. We would like to thank D. O'Callaghan and S. Childs for very helpful discussions on Grid computing. D.F. and G.C.M received funding by the Cosmo Grid project, funded by the Program for Research in Third Level Institutions under the National Development Plan and with assistance from the European Regional Development Fund. This publication makes use of data products from the Two Micron All Sky Survey, which is a joint project of the University of Massachusetts and the Infrared Processing and Analysis Center/California Institute of Technology, funded by the National Aeronautics and Space Administration and the National Science Foundation. This research has made use of the SIMBAD database, operated at CDS, Strasbourg, France.

REFERENCES

Bok, B.J. 1956, AJ, 61, 309
Coghlan, B.A., Walsh, J. & D. O'Callaghan 2005, in 'Advances in Grid Computing - EGC 2005', Peter M.A. Sloot, Alfons G. Hoekstra, Thierry Priol, Alexander Reinefeld, and Marian Bubak, editors, LNCS3470, Amsterdam, The Netherlands, February 2005. Springer.
Draine, B.T. 2003, ARA&A, 41, 241
Froebrich, D., Scholz, A. & Raftery, C.L. 2007, MNRAS, 374, 399
Froebrich, D. & del Burgo, C. 2006, MNRAS, 369, 1901
Froebrich, D., Ray, T.P., Murphy, G.C. & Scholz, A. 2005, A&A, 432, 67
Haas, M., Lemke, D., Stickel, M., Hippelein, H., Kunkel, M., Herbstmeier, U. & Mattila, K. 1998, A&A, 338, 33
Hartmann, L., Ballesteros-Paredes, J. & Bergin, E.A. 2001, ApJ, 562, 852
Lada, C.J., Lada, E.A., Clemens, D.P. & Bally, J. 1994, ApJ, 429, 694
Lombardi, M. 2005, A&A, 438, 169
Lombardi, M. & Alves, J. 2001, A&A, 377, 1023
Mathis, J.S. 1990, ARA&A, 28, 37
Padoan, P., Nordlund, A. & Jones, B.J.T. 1997, MNRAS, 288, 145
Skrutskie, M.F., Cutri, R.M., Stiening, R., et al. 2006, AJ, 131, 1163
Williams, J.P., de Geus, E.J. & Blitz, L. 1994, ApJ, 428, 693
Wolf, M. 1923, AN, 219, 109

APPENDIX A: INDIVIDUAL REGIONS

A1 Extinction and β maps

In the following we show for all individual regions investigated in this paper larger versions of the extinction and β maps. Note that the full resolution FITS file of the extinction map is provided as online material to the paper. We overplot in the maps the position of all known star clusters in the field found in SIMBAD (circles) as well as the new star cluster candidates (+ signs) found in Froebrich et al. (2007), in order to mark regions where potentially the cluster members might dominate the extinction determination (see Sect. 2 for details).

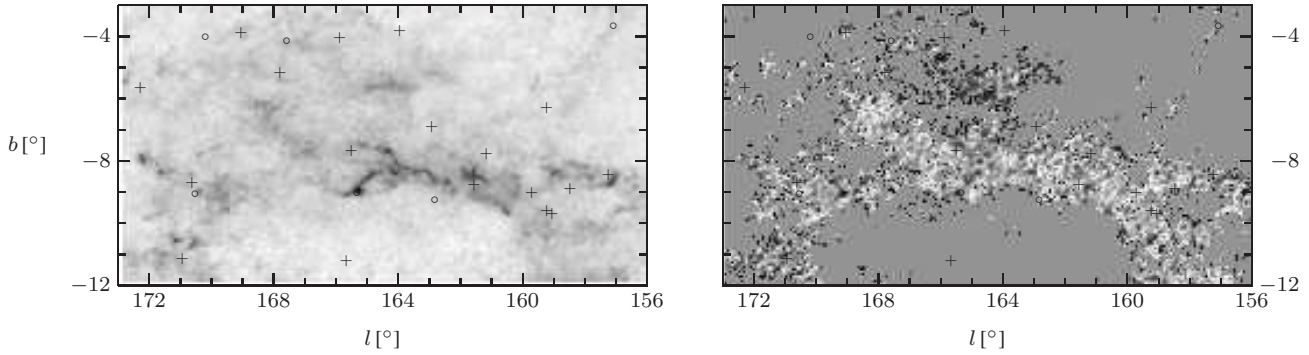


Figure A1. Left panel: Gray scale extinction of the region Auriga 1. Extinction values are scaled linearly from -0.33 to 7 mag of optical extinction. **Right panel:** Gray scale map of β values in the region Auriga 1 for areas where the $\langle J - H \rangle$ and $\langle H - K \rangle$ values are more than 3σ above the noise (for the remaining areas a value of $\beta=1.73$ is adopted). The β values are scaled linearly from zero (black) to three (white). In both panels we indicate the positions of known star clusters from the 2MASS database as circles and from the list from Froebrich et al. (2006) as crosses.

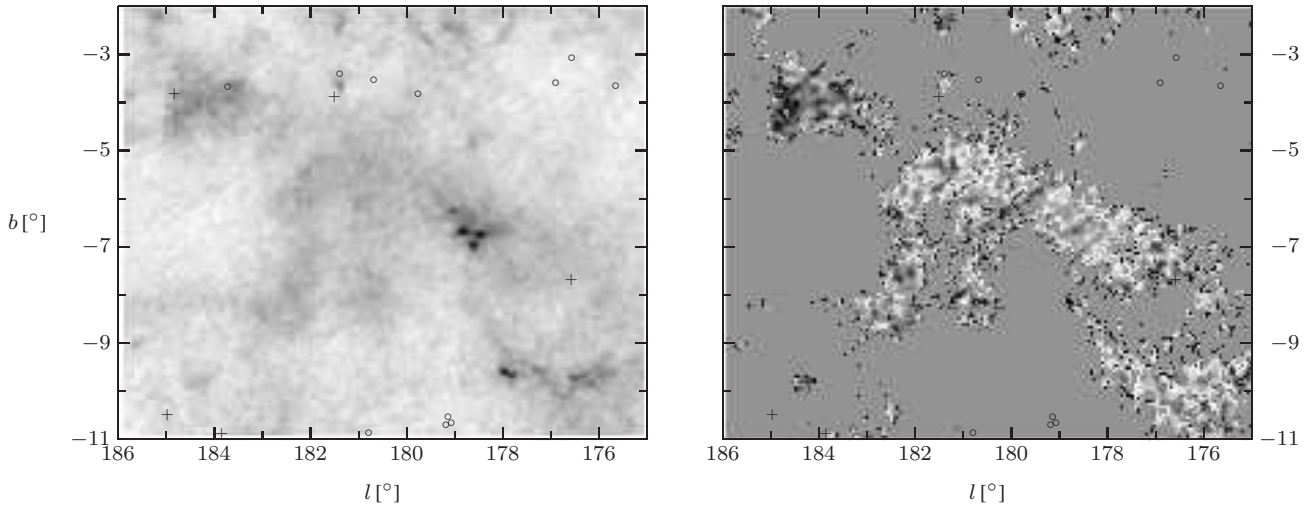


Figure A2. As Fig. A2 but for the region Auriga 2. Extinction values are scaled linearly from -0.33 to 6 mag of optical extinction.

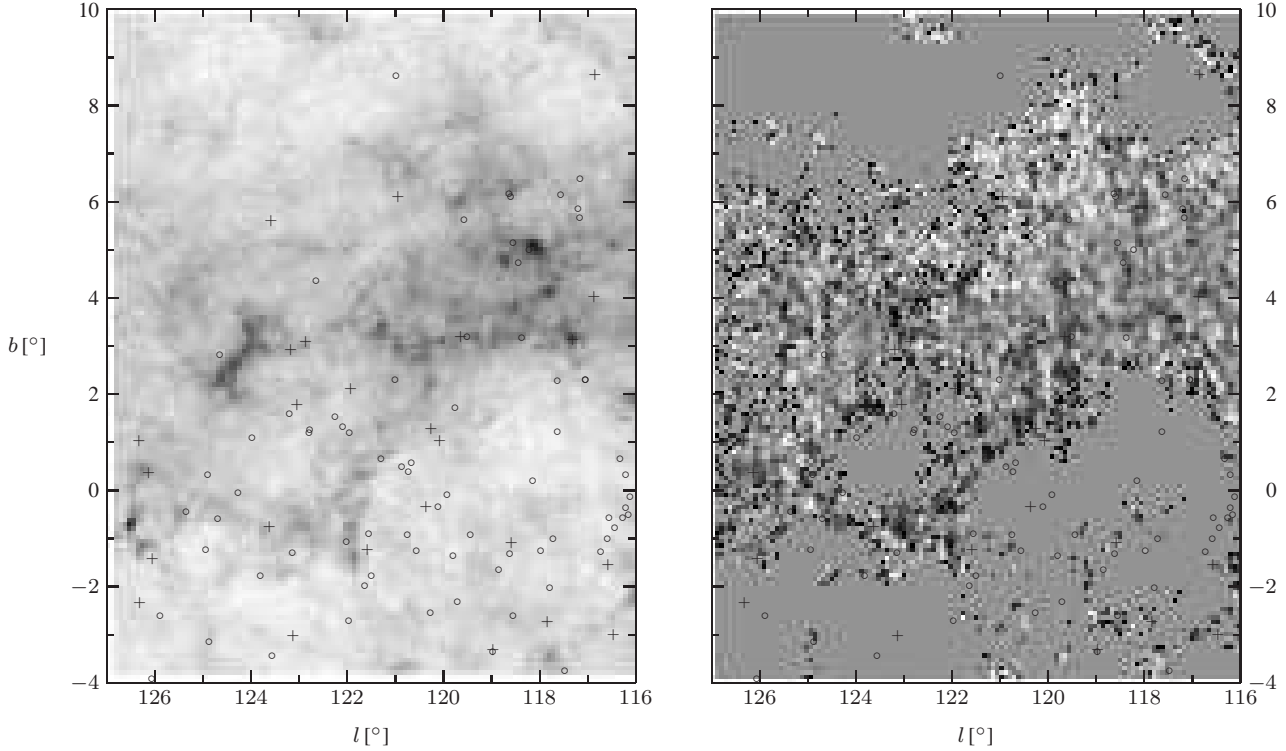


Figure A3. As Fig. A2 but for the region Cassiopeia. Extinction values are scaled linearly from -0.33 to 7 mag of optical extinction.

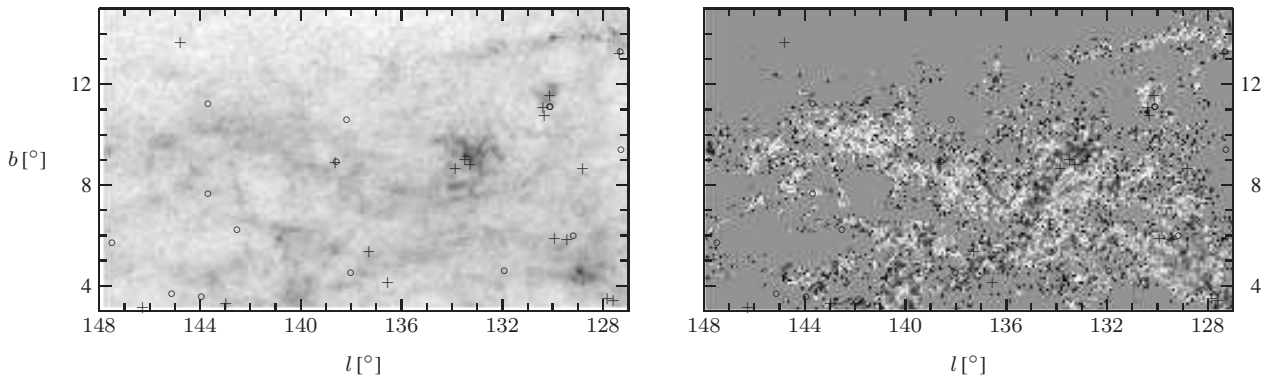


Figure A4. As Fig. A2 but for the region Camelopardalis 1. Extinction values are scaled linearly from -0.33 to 7 mag of optical extinction.

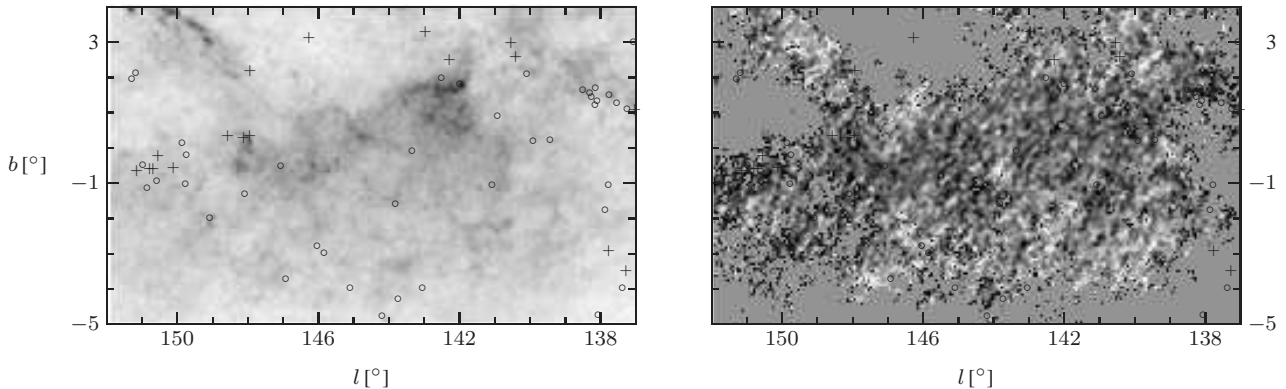


Figure A5. As Fig. A2 but for the region Camelopardalis 2. Extinction values are scaled linearly from -0.33 to 8 mag of optical extinction.

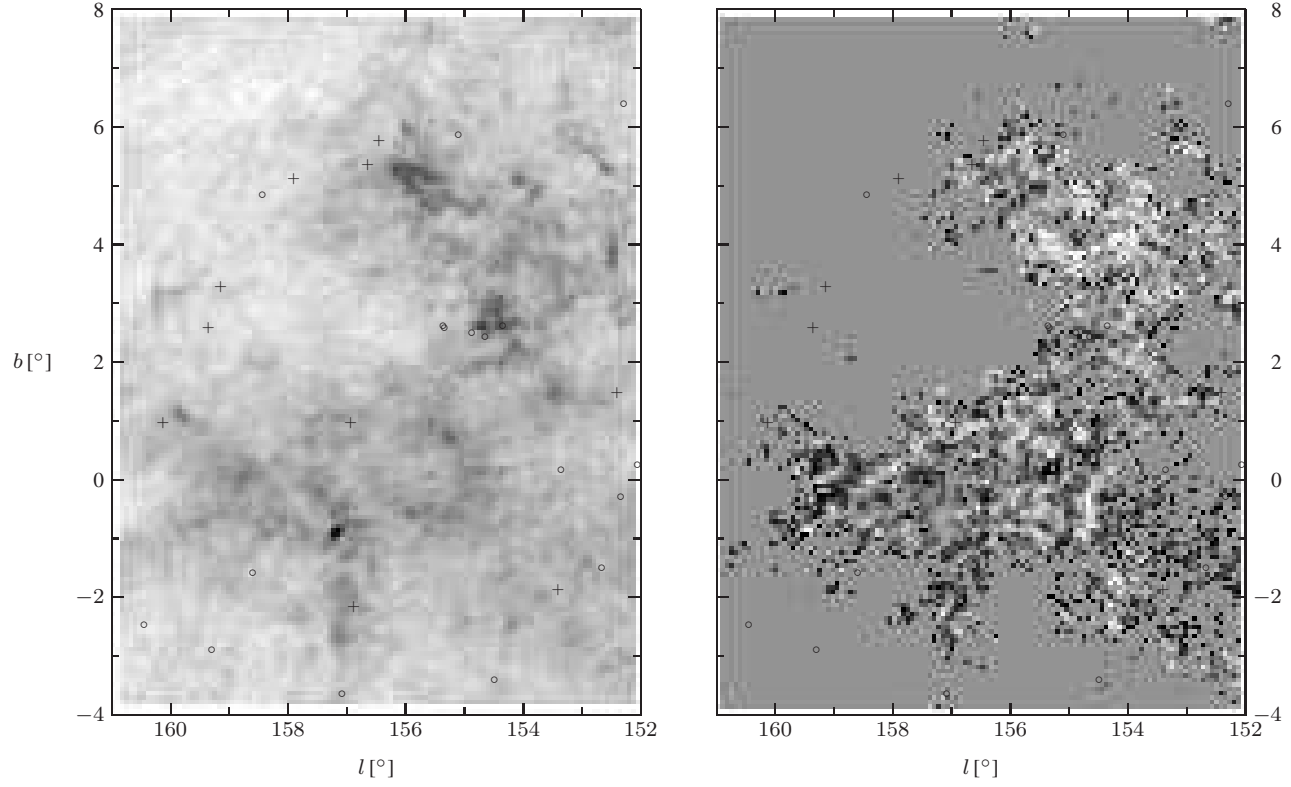


Figure A6. As Fig. A2 but for the region Camelopardalis 3. Extinction values are scaled linearly from -0.33 to 5 mag of optical extinction.

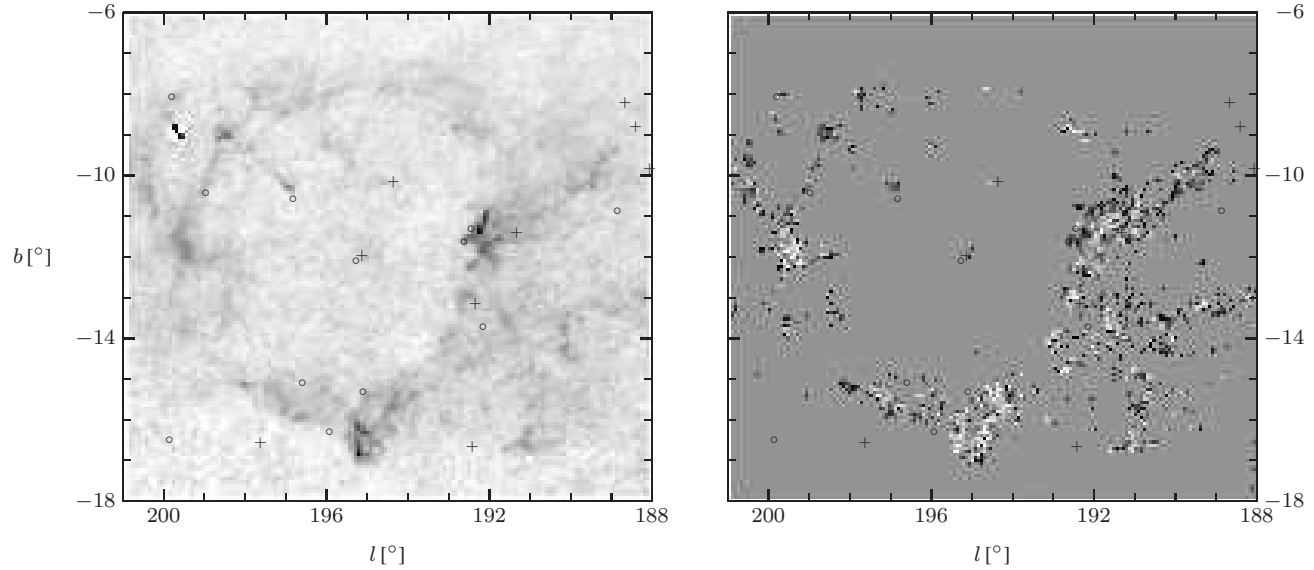


Figure A7. As Fig. A2 but for the region λ -Ori. Extinction values are scaled linearly from -0.33 to 6 mag of optical extinction.

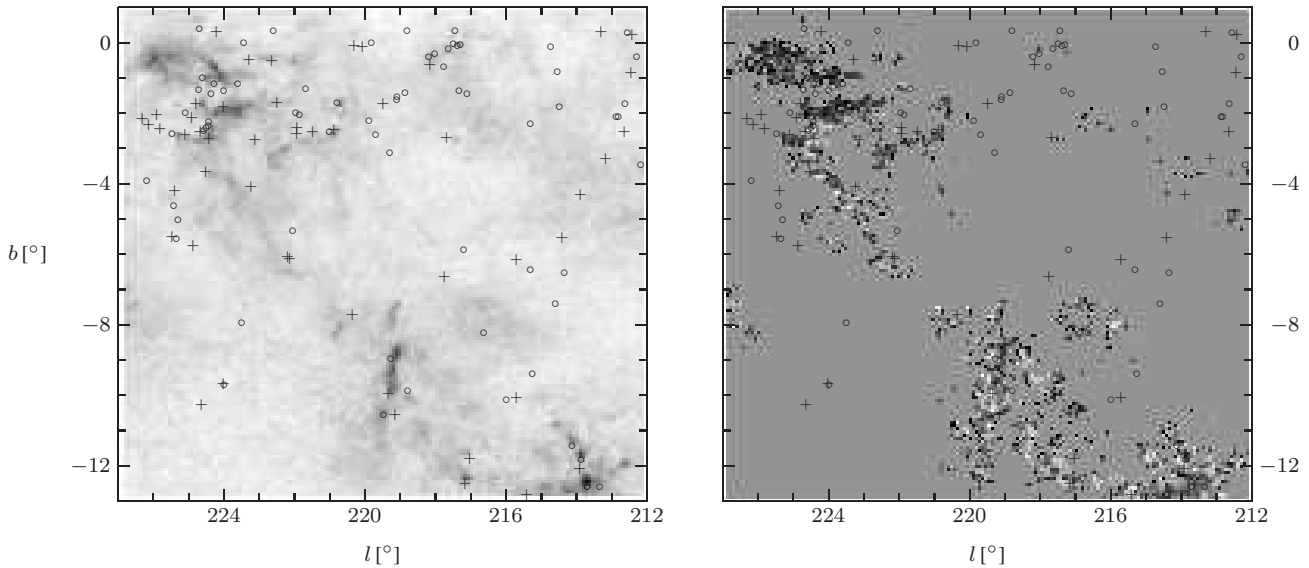


Figure A8. As Fig. A2 but for the region Monoceros. Extinction values are scaled linearly from -0.33 to 7 mag of optical extinction.

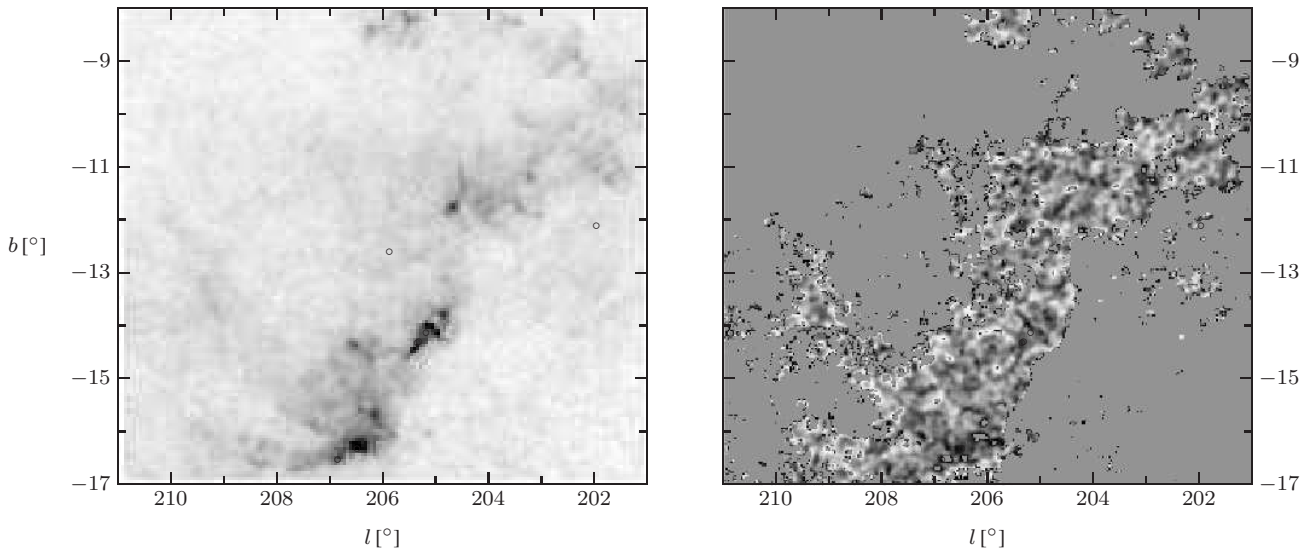


Figure A9. As Fig. A2 but for the region Ori B. Extinction values are scaled linearly from -0.33 to 10 mag of optical extinction.

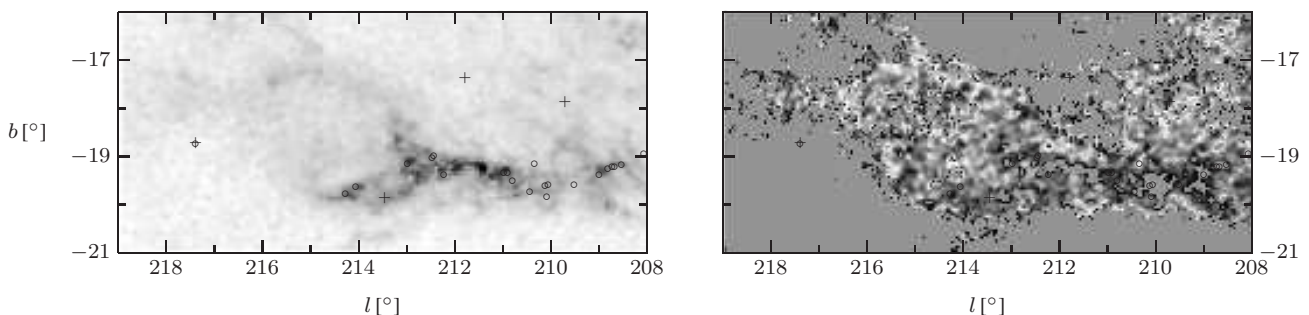


Figure A10. As Fig. A2 but for the region Ori A. Extinction values are scaled linearly from -0.33 to 12 mag of optical extinction.

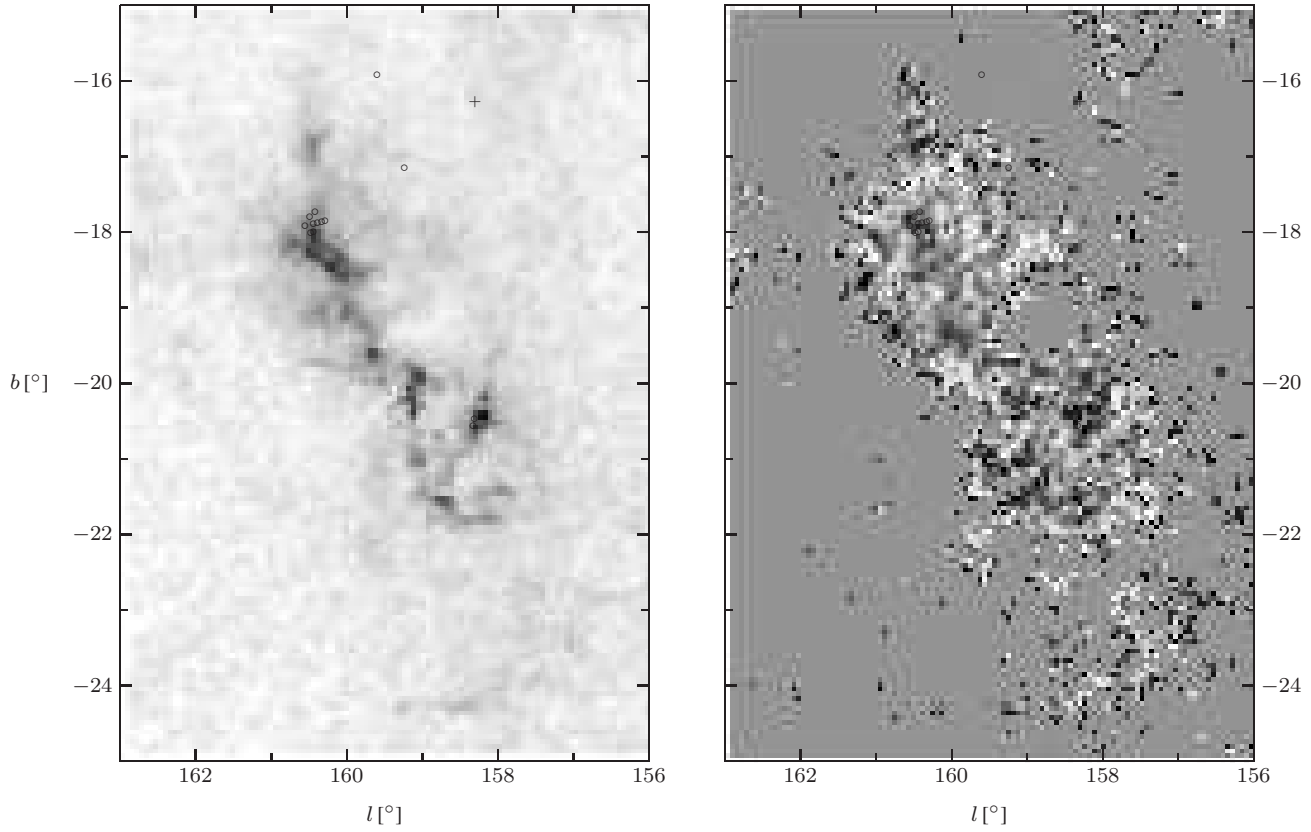


Figure A11. As Fig. A2 but for the region Perseus. Extinction values are scaled linearly from -0.33 to 10 mag of optical extinction.

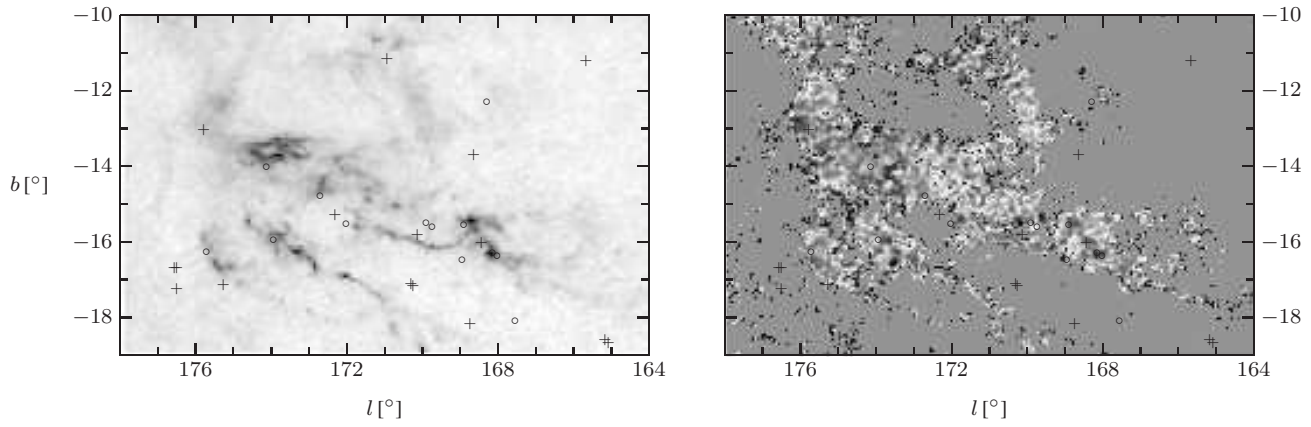


Figure A12. As Fig. A2 but for the region Taurus. Extinction values are scaled linearly from -0.33 to 12 mag of optical extinction.

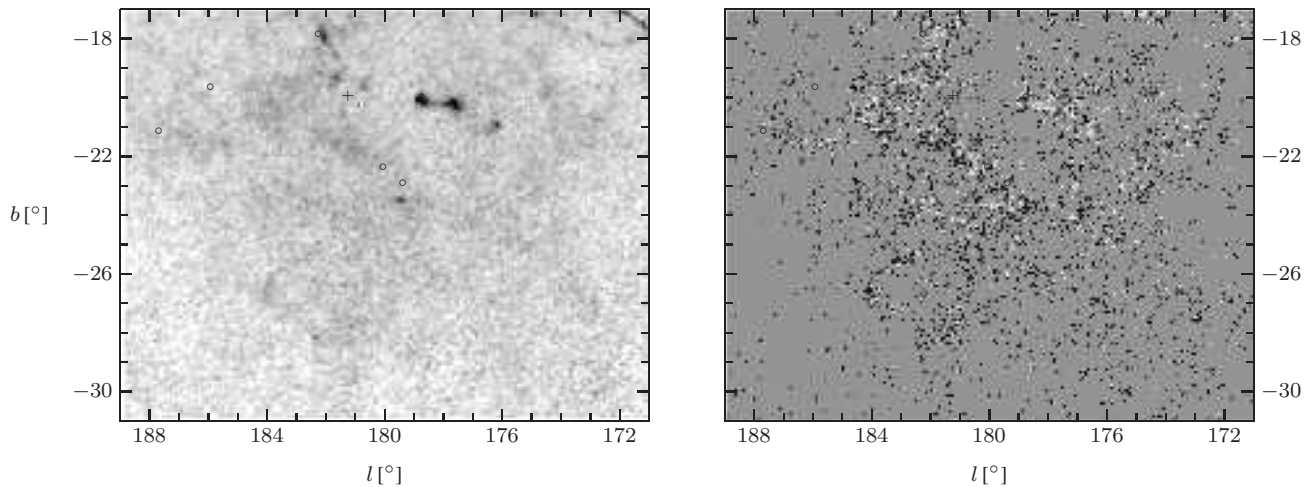


Figure A13. As Fig. A2 but for the region Taurusextended. Extinction values are scaled linearly from -0.33 to 5 mag of optical extinction.

A2 β and column density distributions

In the following we show for all individual regions investigated in this paper the distribution of β and column density values.

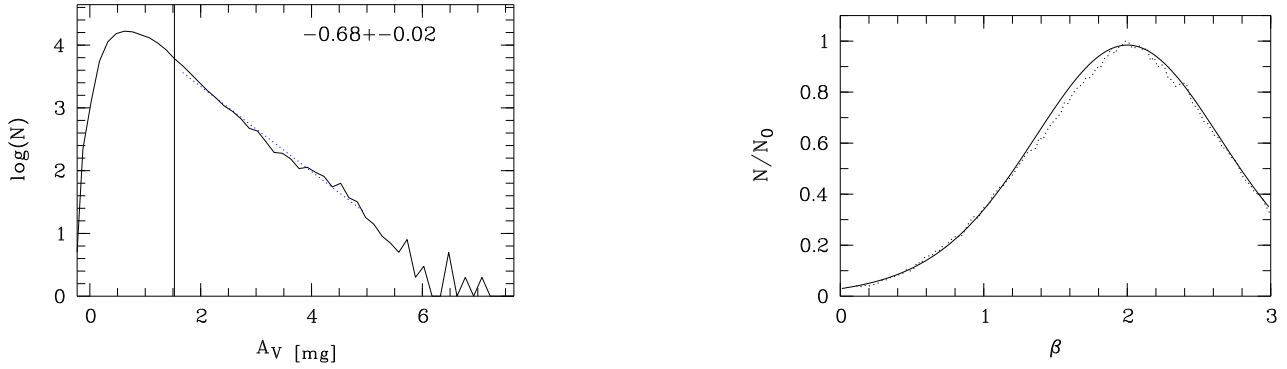


Figure A14. Left: Measured column density distribution in the region Auriga 1 (solid line). As dashed lined we overplot the linear fit to the area above the 5σ noise level (vertical line). The slope of this fit is indicated in the graph. **Right:** Measured distribution of β values in the region Auriga 1 (dotted line) and overplotted model prediction for the assumption of a single β value with internal scatter in the entire region. The measured distribution includes only pixels where the $< J - H >$ and $< H - K >$ values are more than 3σ above the noise.

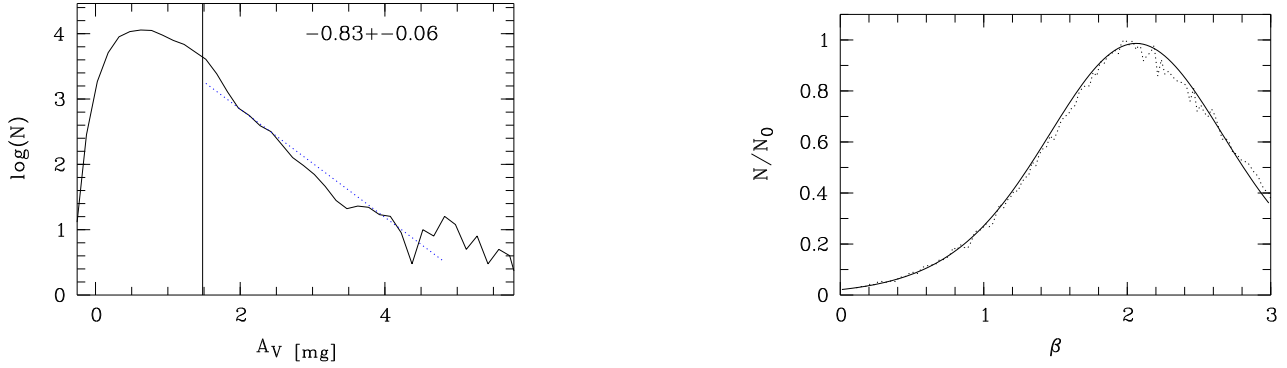


Figure A15. As Fig. A14 but for region Auriga 2.

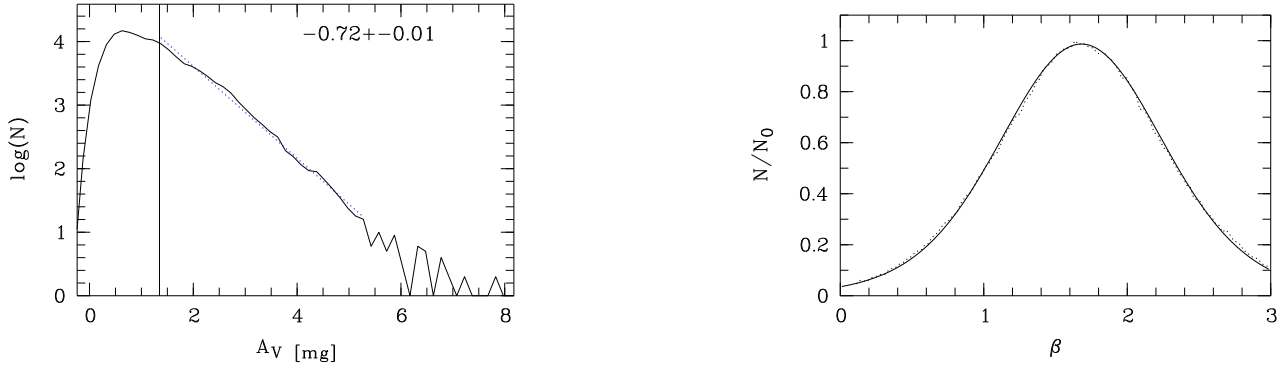


Figure A16. As Fig. A14 but for region Cassiopeia.

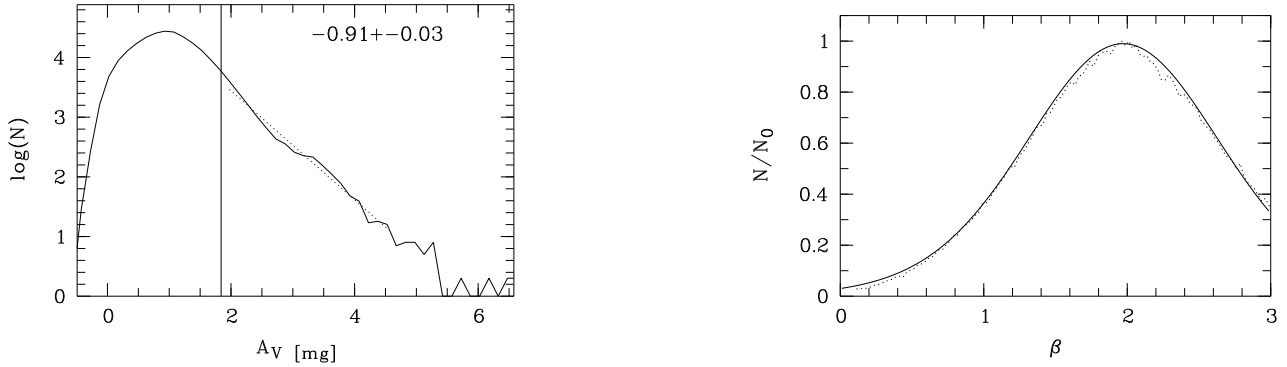


Figure A17. As Fig. A14 but for region Camelopardalis 1.

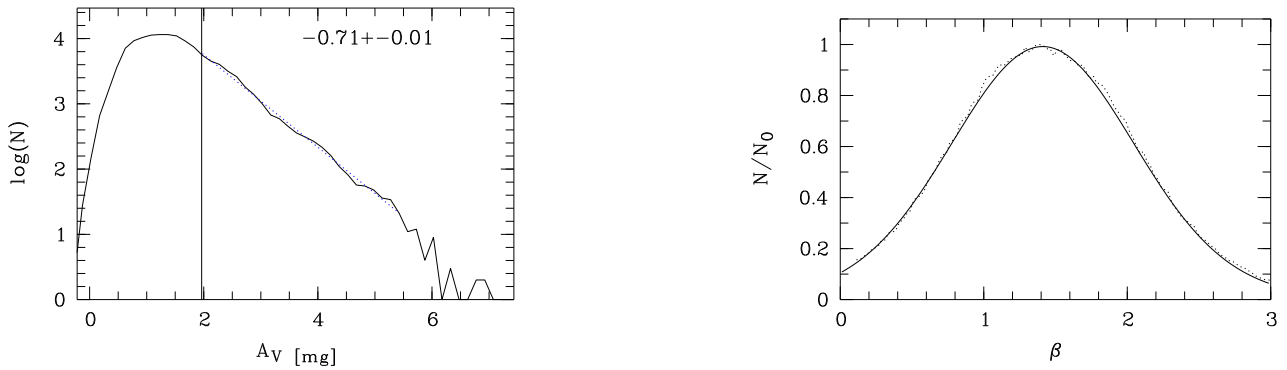


Figure A18. As Fig. A14 but for region Camelopardalis 2.

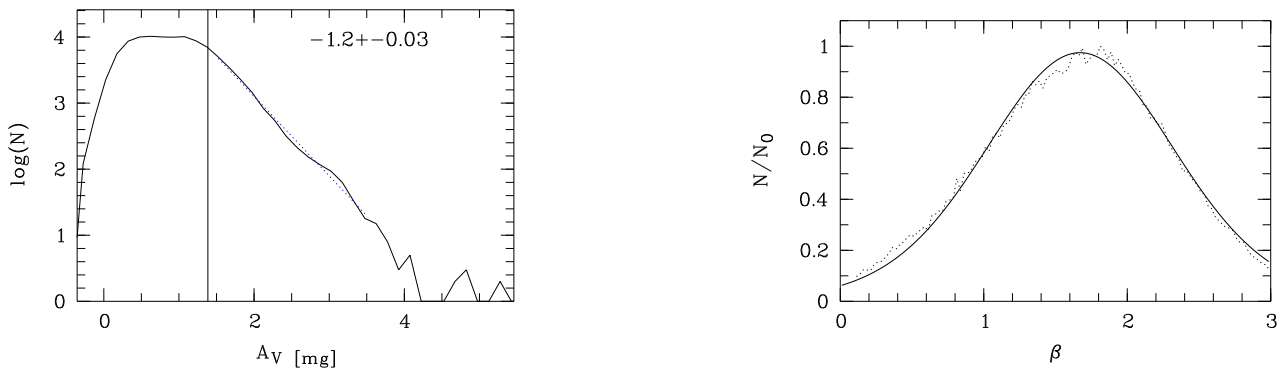


Figure A19. As Fig. A14 but for region Camelopardalis 3.

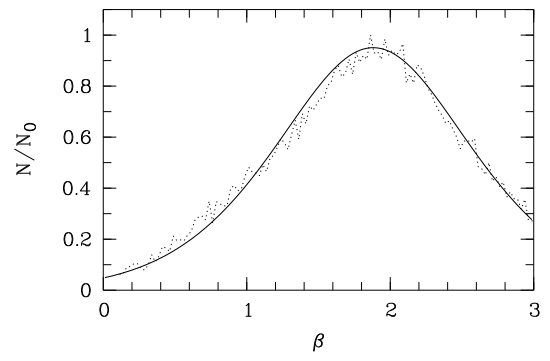
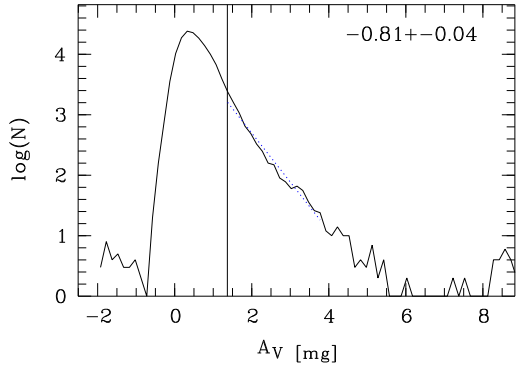


Figure A20. As Fig. A14 but for region λ -Ori.

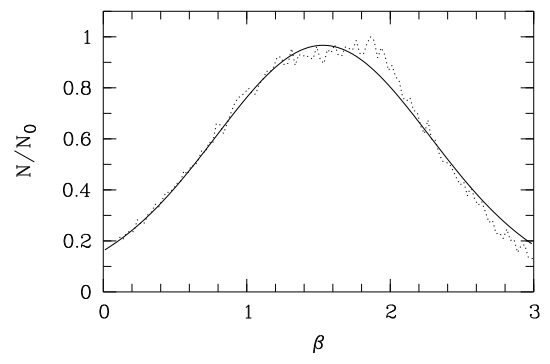
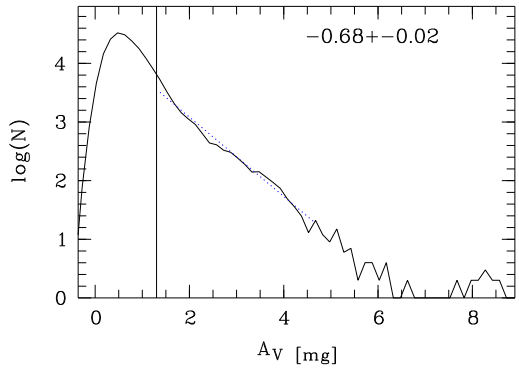


Figure A21. As Fig. A14 but for region Monoceros.

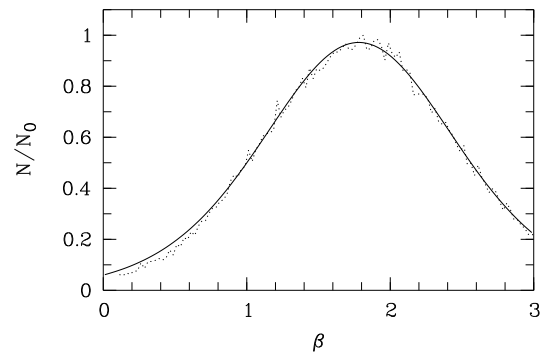
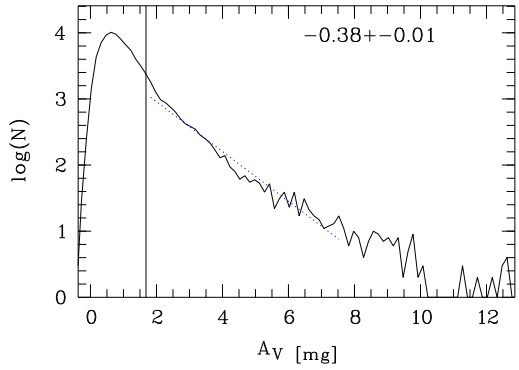


Figure A22. As Fig. A14 but for region Ori B.

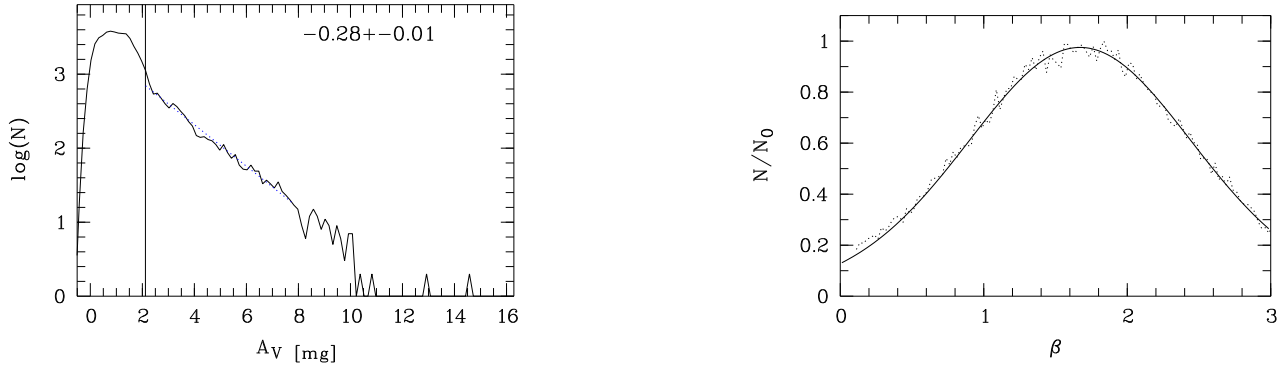


Figure A23. As Fig. A14 but for region Ori A.

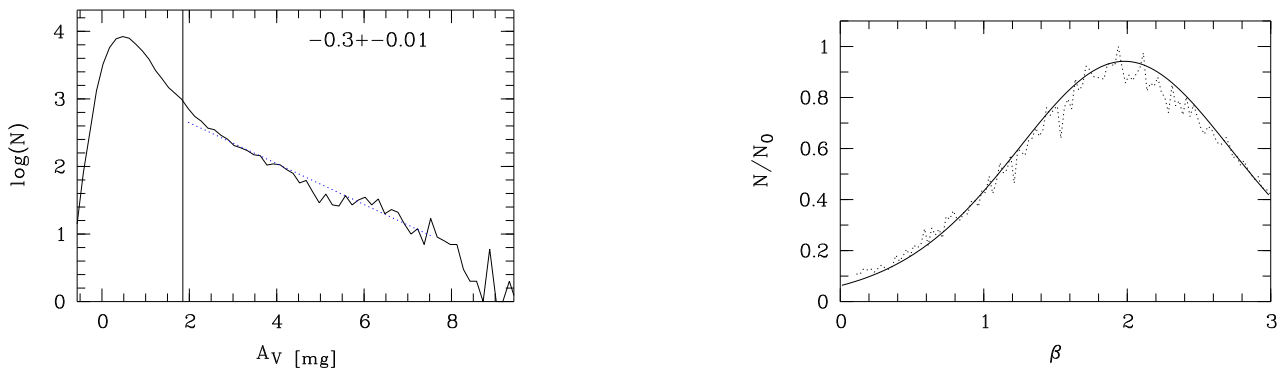


Figure A24. As Fig. A14 but for region Perseus.

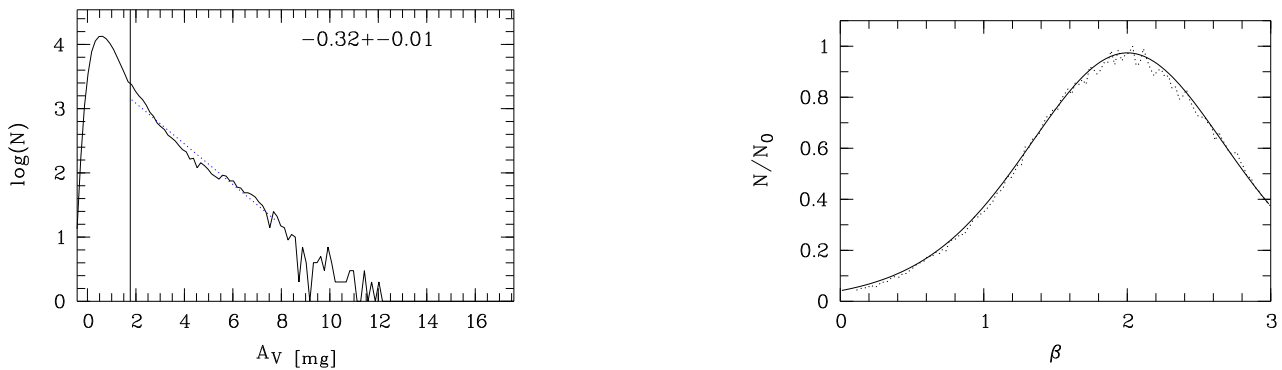


Figure A25. As Fig. A14 but for region Taurus.

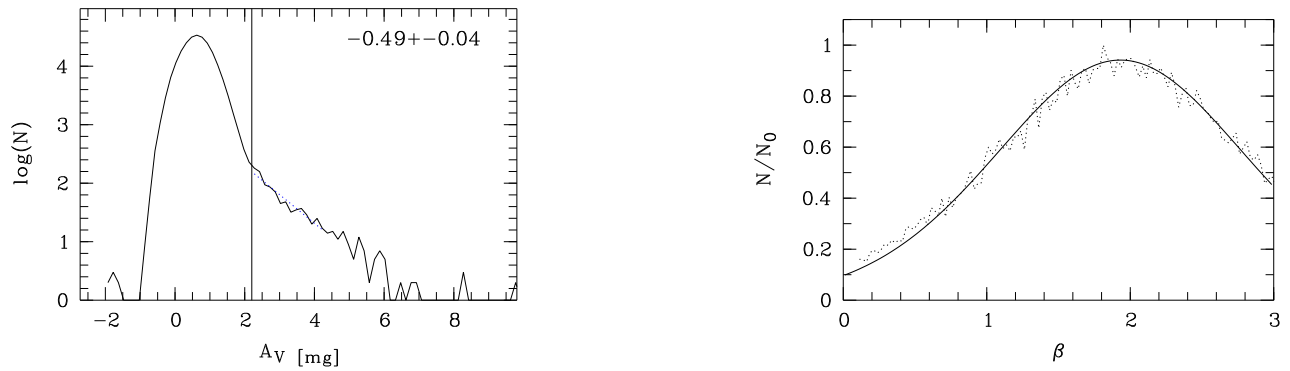


Figure A26. As Fig. A14 but for region Taurusextended.